

UC San Diego

UC San Diego Previously Published Works

Title

Constructing 2D maps of human spinal cord activity and isolating the functional midline with high-density microelectrode arrays

Permalink

<https://escholarship.org/uc/item/98g6c7fj>

Journal

Science Translational Medicine, 14(664)

ISSN

1946-6234

Authors

Russman, Samantha M
Cleary, Daniel R
Tchoe, Youngbin
[et al.](#)

Publication Date

2022-09-28

DOI

10.1126/scitranslmed.abq4744

Peer reviewed



HHS Public Access

Author manuscript

Sci Transl Med. Author manuscript; available in PMC 2022 November 11.

Published in final edited form as:

Sci Transl Med. 2022 September 28; 14(664): eabq4744. doi:10.1126/scitranslmed.abq4744.

Constructing 2D Maps of Human Spinal Cord Activity and Isolating the Functional Midline with High-Density Microelectrode Arrays

Samantha M. Russman^{1,2}, Daniel R. Cleary^{2,3}, Youngbin Tchoe², Andrew M. Bourhis², Brittany Stedelin⁴, Joel Martin^{2,3}, Erik C. Brown⁴, Xinlian Zhang⁵, Aaron Kawamoto⁴, Won Hyung A. Ryu⁴, Ahmed M. Raslan⁴, Joseph Ciacci³, Shadi A. Dayeh^{1,2,*}

¹Department of Bioengineering, University of California San Diego, La Jolla CA, 92093, USA

²Integrated Electronics and Biointerfaces Laboratory, Department of Electrical and Computer Engineering, University of California San Diego, La Jolla CA, 92093, USA

³Department of Neurosurgery, University of California San Diego, La Jolla CA, 92093, USA

⁴Department of Neurosurgery, Oregon Health & Science University, Portland, Oregon, 97239

⁵Division of Biostatistics and Bioinformatics, Herbert Wertheim School of Public Health, University of California San Diego, La Jolla CA, 92093, USA

Abstract

Intraoperative neuromonitoring (IONM) is a widely used practice in spine surgery for early detection and minimization of neurological injury. IONM is most commonly conducted by indirectly recording motor and somatosensory evoked potentials from either muscles or the scalp, which requires large-amplitude electrical stimulation and provides limited spatiotemporal information. IONM may inform of inadvertent events during neurosurgery after they occur, but it does not guide safe surgical procedures when the anatomy of the diseased spinal cord is distorted. To overcome these limitations and to increase our understanding of human spinal cord neurophysiology, we applied a microelectrode array with hundreds of channels to the exposed spinal cord during surgery and resolved spatiotemporal dynamics with high definition. We used this method to construct two-dimensional maps of responsive channels and define with submillimeter precision the electrophysiological midline of the spinal cord. The high sensitivity of our microelectrode array allowed us to record both epidural and subdural responses at stimulation currents that are well below those used clinically and to resolve post-operative evoked potentials when IONM could not. Taken together, these advances highlight the potential

*Corresponding author. sdayeh@eng.ucsd.edu.

Author contributions: S.A.D., J.C., D.R.C. and J.M. conceived project which was refined by input from A.M.R. and W.H.A.R.; S.A.D. led all aspects of the project. S.M.R. fabricated the grids, designed the tasks, and conducted all data analysis with S.A.D.'s guidance and with input from Y.T. S.M.R. performed statistical analysis with input from X.Z. S.M.R., D.R.C., A.M.B, B.S., J.M., E.B., A.K., W.H.A.R., A.M.R. J.C., and S.A.D. performed recordings in the operating room. S.A.D. and S.M.R. wrote the manuscript and all authors discussed the results and contributed to the manuscript writing.

Competing Interests: The authors declare the following competing interests. Y.T., A.M.R. and S.A.D. have equity in Precision Neurotek Inc. that is co-founded by the team to commercialize PtNRGrids for intraoperative mapping. S.A.D. has competing interests not related to this work including equity in FeelTheTouch LLC. S.A.D. was a paid consultant to MaXentric Technologies. D.R.C. has equity in Surgical Simulations, LLC. A.M.R. has an equity and is a cofounder of CerebroAI. AMR received consulting fees from Abbott Inc and Biotronik Inc.

of our microelectrode arrays to capture previously unexplored spinal cord neural activity and its spatiotemporal dynamics at high resolution, offering better electrophysiological markers that can transform IONM.

One Sentence Summary:

Generation of two-dimensional maps of human spinal cord activity using high-channel count surface microelectrode arrays

INTRODUCTION

Spinal surgeries most often work around the spinal cord, nerve roots, and associated blood vessels, with some cases requiring entry into the neural elements. In either case, surgery has an inherent risk for debilitating or devastating postoperative neurological deficits (1–4). For surgery involving the spinal cord and nerves, this risk is particularly profound when a safe entry or dissection pathway cannot be readily identified, such as when resecting intradural spinal cord tumors (5). For surgeries with risk of neurological injury, the surgeons will often use intraoperative neurophysiological monitoring (IONM) of the spinal cord to indirectly assess the functional integrity of motor and sensory pathways when operating in or around spinal neural structures.

IONM has previously been shown to improve surgical outcomes (1–4, 6–10), but in its current form, it only provides an indirect evaluation of the structural and functional spinal pathways. During IONM, somatosensory evoked potentials (SSEPs) are recorded from the scalp in response to electrical current stimulation of a peripheral nerve, and motor evoked potentials (MEPs) (11–15) are recorded from the upper and lower limb muscles in response to transcranial electrical stimulation (TES) (16–19). In recording SSEPs from the brain, the scalp, cranium, and dura all act as insulators resulting in low amplitude responses. As a result, high-amplitude stimulation currents must be applied with high-count stimulation trains to improve signal-to-noise ratio of the averaged recordings and extract electrophysiological signals from the recording system's baseline noise (19–21). These stimulation trains also prevent real-time monitoring, where neurological injuries may not be noticeable for many minutes after the triggering event (22). Finally, the physical separation of the recording contacts on the scalp from the surgical site on the spinal cord prevents recording of spatiotemporal, anatomical, and physiological features of responses.

IONM is also not without controversies. The sensitivity and specificity of SSEP and MEP are not perfect, where false positives may lead to cessation of surgery and incomplete resection, false negative may lead to undetected injury (23–25). Additionally, there is still the practice of wake-up testing in certain spine surgeries such as scoliosis. Additionally, SSEPs may not change if the injury is purely motor or vascular.

We hypothesized that direct recording of SSEPs by microelectrodes on the surface of the spinal cord could increase the fidelity of these recordings and reduce the number of required trials, allowing real-time spatiotemporal mapping. We also predicted that recordings with a high channel count microelectrode array would offer two dimensional (2D) SSEP responses,

which would allow for more precise identification of the spinal cord functional midline at the point of resection. The functional midline is the only safe corridor to the inner structure of the spinal cord; therefore, its identification is of critical relevance. Unfortunately, there is no consistent or accurate anatomic landmark to the midline on the surface and moreover, it is often distorted with tumors/masses or rotated due to adhesions. Precise functional midline identification would be advantageous given that the position of the anatomical and functional midline has been found to be mismatched by up to 2 mm in 40% of patients (26, 27). Dorsal column (DC) mapping in spinal cord surgery was shown to decrease the occurrence of new postoperative sensorimotor dysfunction by 42% (28). There are limited studies that reported DC mapping by recording SSEPs directly from the surface of the spinal cord using linear 8-contact arrays (29, 30). In these studies, sparse mapping of the midline was performed by direct electrical stimulation of the dorsal column using a linear array of 8 contacts made of Teflon-coated stainless-steel wires that were 76 μm in diameter and 1 mm apart. The midline was identified by phase reversal in the recorded SSEPs. In two other studies, SSEPs were stimulated from the spinal cord surface and recorded from the brain, again identifying a rudimentary functional midline (31, 32).

We fabricated high-channel number microelectrode arrays by leveraging low-impedance contact materials we have used before in cortical recordings such as poly(3,4-ethylenedioxythiophene) polystyrene sulfonate (PEDOT:PSS) (33–36) and platinum nanorod (PtNR) (37) contacts. Our electrodes were fabricated on thin ($\sim 6.6 \mu\text{m}$) parylene C substrates (38, 39), which allowed for high conformability to the pial surface of the spinal cord during IONM. We observed dynamic patterns of ipsilateral and contralateral SSEPs with high-resolution that allowed us to identify a microscale midline boundary. This high-resolution boundary was identified at clinical stimulation currents and persisted even when scalp SSEPs could not be identified. Our microelectrode array also outperformed clinical equipment given that our recordings were directly on the spinal cord surface and thus did not require substantial trial averaging. In the future, this technology could provide a practically instantaneous IONM method once data analysis and plotting are incorporated in real-time. Taken together, our microelectrode grid can improve IONM and could have other applications, such as for evaluation or even treatment of spinal cord injury (SCI).

RESULTS

Experiment design and surgical implantation

To assess the viability of recording spatiotemporal SSEP patterns with high quality and resolution from the surface of the spinal cord, we recorded SSEPs with a high-density microelectrode array in subjects ($N=6$) undergoing intramedullary tumor or biopsy procedures in the cervical spinal cord (Fig. 1A). The microelectrode array recordings were adjunct to the surgery, completed with minimal disruption to the surgical flow of the procedure time and performed with institutional review board (IRB) authorization at the University of California San Diego and at Oregon Health & Sciences University. The microelectrode array recordings were performed during three timepoints in the surgery: epidurally and subdurally before tumor resection or biopsy and subdurally post-resection or biopsy. The electrode was placed on the exposed surface spinal cord for tumor resection,

covered the DCs and was centered over the anatomical midline of the spinal cord. That surface placement spanned an apparently normal areas of the spinal cord rostral and caudal to the lesion. The placement was documented with intraoperative photos from the surgical microscope. Suction and sponges were used to remove excess blood and cerebrospinal fluid (CSF) from the spinal cord surface to ensure good electrode-tissue contact during the recordings (Fig. 1B). Suction and sponges near the electrode did not negatively impact recording quality or introduce substantive noise into the data.

Electrode design

Multiple electrode designs were used in the recordings from the six subjects (Table S1), with results presented in this work from subjects 4–6. Recordings from these subjects used a single electrode design and leveraged a long, high-density connector that was not available for the earlier subjects (Fig. 1C). Additionally, the overall width of the electrode was reduced from 1.6 cm to 6.4 mm in the final design to maintain stable contact with the dorsal column and account for variable width of the surgical area. These subjects were temporarily implanted with a microelectrode array with 372 PtNR contacts (diameter=30 μm) arranged in a rectangular array of 12 \times 31 with 350 μm horizontal (circumferential) pitch and 400 μm vertical (axial) pitch providing a coverage area of $3.85 \times 12 \text{ mm}^2$. At the tip of the array, an additional 54 contacts of variable diameter in the range of 30 μm – 480 μm were arranged in clusters of three contacts per diameter on the left and right sides of the array. The goal of the multidiameter array was to validate the effectiveness of small contact sizes in recording high quality SSEPs.

The electrodes were designed to have a sterile/non-sterile interface junction along a long connector board (Fig. 1C) to facilitate the use of these devices in the operating room (OR). Whereas the whole thin film device and extender board of Fig. 1C were sterilized at the hospital before use, the extender board separated the recording electronics board from the sterile area, allowing it to be encased in a sterile bag, thus maintaining an overall sterile field in the OR. Additional details on packaging, sterilization, and OR use have been previously reported (40).

Our 6.6 μm parylene-C microelectrode arrays were much thinner than current clinical spinal cord grids (Fig. 1D, 1 mm thick silicone), therefore more conformal to the spinal surface and compliant to movement during recording. Additionally, the microelectrode arrays were transparent, which gave the surgeon an unobstructed view of the surface spinal anatomical features when the grid was in place. The 1kHz electrochemical impedance of the microelectrode array used in subject 5 measured in phosphate buffered saline post-fabrication was $22.77 \pm 15.11 \text{ k}\Omega$. The impedance values did not change significantly ($p=0.5926$) after Sterrad sterilization, a hydrogen peroxide gas plasma technology which is compatible with the PtNRGrids (40), and were $23.24 \pm 5.42 \text{ k}\Omega$ post-sterilization (Fig 1E). On the pial surface, the contacts exhibited slightly higher impedance values, with a mean of $35.82 \pm 14.21 \text{ k}\Omega$, an increase that is expected when measuring on tissue (41). These impedance values are representative of those measured across subjects 4–6 (Fig. S1). Our recording analysis focused on microelectrode contacts that exhibited a 1kHz impedance lower than 120 $\text{k}\Omega$ as recordings with contacts with higher impedances are susceptible

to noise. After fabrication, sterilization and throughout multiple surgical placements and recordings, our microelectrode arrays maintained a yield above 87% (Fig. 1E, Fig. S1). These measurements show the stability of the microelectrode array throughout sterilization and all experimental procedures.

Stimulation paradigm

The IONM team delivered electrical stimulation to both upper limb (typically median) and lower limb (typically tibial) nerves in trains of 40 at 2.78 Hz. Stimulation current amplitudes were initially set to clinical amplitudes used by the IONM team between 30 mA – 50 mA depending on the subject. The stimulation amplitudes were then decreased to $\frac{1}{2}$, $\frac{1}{4}$, and $\frac{1}{8}$ of these clinical amplitudes. For subject 5, the current amplitudes used were therefore 30, 15, 7.5 and 4 mA, which was the lowest current amplitude used for stimulation across all patients.

Response amplitudes and thresholds

For both epidural and subdural placements, SSEPs had an onset latency of 10 ms and peak latency of ~ 12 ms (Fig. 1F, Fig. 2A–D). This is consistent with previous recordings with low-channel count microgrids from the surface of the spine (11, 42, 43). Averaged maximal peak-to-peak SSEP amplitudes ranged from 8–10 μV for 30 mA stimulation to ~ 1 μV for 4 mA stimulation for 30–40 trials. Representative channels with high response amplitudes are shown in Figure 1F. Statistical analysis was used to evaluate whether the peak-to-peak amplitudes were statistically significant compared to pre-stimulus baseline. This was in particular a question for low stimulation currents where the signal to noise ratio was low, which we classified as below $\text{SNR} = 6$ (Table 1). A Mann Whitney U test showed significance at almost all current amplitudes at $p < 0.001$ (Table 1). However, for 4 mA current amplitudes in both epidural and subdural placements, the effect size was equal to or less than 1, indicating that any differences may not be observable or clinically relevant. A similar low effect size of -1.15 was observed for 15 mA left subdural recording, which we suspect was caused by a fluid build-up on the spinal cord leading to poor electrode-tissue contact for this stimulation amplitude. Generally, for high current amplitudes, response amplitudes were significant (p-values can be found in Table 1) for both epidural and subdural placements. Overall, these results indicate that both placements are appropriate for detection of neural signals.

During each case, we also performed a control recording on skin to confirm that the changes in voltage we observed were due to neural activity and not the stimulation artifact. In this subject, the peak-to-peak amplitudes of skin recordings at the clinical stimulation amplitude were below 1 μV (mean = 0.56 ± 0.18 μV), which was lower compared to the baseline (mean = 0.75 ± 0.24 μV) (Fig S2). Similar patterns were observed among all subjects.

Spatiotemporal response patterns

Our microelectrode array was placed on the spinal cord allowing it to capture spatiotemporal features of the SSEPs, which current IONM clinical equipment cannot resolve because the recording electrodes are placed on the surface of the scalp. Whereas amplitudes of the responses were similar between the epidural and subdural placements, subdural recordings

were more localized, especially for higher current amplitudes where response amplitude varied substantially across the array (Fig. 2A–D). Epidural recordings showed more uniform responses across channels compared to subdural recordings, which manifested in a wider spread of responses across the array. Spatiotemporal profiles of subdural recordings showed similar patterns in response propagation for different stimulation currents. A plot of peak-to-peak responses for all current amplitudes calculated from these time evolution plots is shown in Fig. S3. These response patterns and dependencies on stimulation currents are consistent with recordings from other subjects (Figs. S4–S5). Higher response amplitudes were registered on the side of the body where the stimulation was delivered; left channels were more responsive for left median nerve stimulation and right channels for right median nerve stimulation. This is consistent with spinal cord anatomy as the DCs are largely ipsilateral to the peripheral nerves entering the spine.

The conduction velocity of the SSEPs was calculated from the approximate distance of the median nerve stimulating electrode to the recording microelectrode and the peak latency. This was found to be 50 ± 4.5 m/s assuming an arm length of 0.6 m. Previous reports provide conduction velocities in the range of 91.3 ± 7.2 m/s for A α nerve fibers (44) and 63.4 ± 4.5 m/s (45) and 69.3 ± 6.6 m/s for A β nerve fibers, which carry sensory information (46). Our lower estimated conduction velocity might be explained by errors in estimation of arm length and the synapsing of the nerve fibers onto interneurons in the spinal cord. Our calculated SSEP and the onset time of the response could be used to assess neurological damage since changes over 10% in onset latency in clinically recorded scalp SSEPs are considered a sign of spinal cord dysfunction (47).

Mapping of the functional midline

The anatomical spinal cord midline in normal tissue can be identified anatomically by the dorsal median sulcal vein as it enters the midline raphe or at the middle point between the root entry zones on either side of the cord (29). This anatomical midline can be distorted by tumors, edema, neovascularization, or scar formation, prohibiting its identification using anatomical landmarks. To prevent inadvertent dissection of the DCs, which can result in postoperative morbidity that can be disabling, functional mapping is used to locate the midline to inform the spinal incisions (myelotomy). Using the spatiotemporal features of the recorded SSEPs, we performed analysis to map the functional midline for epidural and subdural recordings pre-resection and subdural recordings post-resection. The midline was identified with better precision in the subdural recording, which is consistent with the more localized response profiles for this placement. By tuning the thresholding method for positive responses and their amplitudes as described in the Methods section, we were able to isolate ipsilateral responses to stimulation and outline a midline spanning 2–5 channels equivalent to a distance of 700 μ m to 1.75 mm (Fig. 2F). This mapping is of higher resolution than reported previously with the use of 8-channel microgrids (29, 30), where their contact spacing were equal to or larger than 1 mm. Additionally, with our microelectrode, the midline can be traced in the rostrocaudal direction, which cannot be done with the linear microgrid. The epidural functional midline was difficult to define given the large spread of the responses (Fig. 2E). These results were consistent in subject 4 (Fig. S6). We were not able to identify the midline in patient 6 given the positioning of the

electrode and tumor effects (Fig. S7). Subdural post-resection placement also allowed for identification of the functional midline, which is described in a later section. These results show that subdural placement allows mapping of the functional midline.

Spatial phase gradient analysis of response propagation

We performed an analysis of the spatial phase gradient of the response to better understand response propagation. We calculated the phase gradients and overlaid streamlines for better visualization of wave propagation dynamics. We hypothesized that the neural responses originate from a bundle of axons deep within the spinal cord, and therefore we would expect to see the electric field lines aligned parallel to the axons generating action potentials, dropping off in strength radially from the center of these axons (48). The microelectrode array captures the 2D projection of these electric field lines along the surface of the spinal cord. Furthermore, since the neural response is propagating vertically in a rostral direction, the electric field strength will also vary as a function of time. Thus, the spatial phase gradient should primarily point in the direction of the traveling action potentials, though due to the complex nature of the 2D projected electric field lines, will also spread outward from the center of the response in the direction of decreasing electric field strength. We observed these phase gradient features in the subdural pre-resection and to a lesser extent in the post-resection recordings (Fig. 3). Post-resection recordings will be discussed below. We did not see a strong directionality of the phase gradient in the epidural recordings, which can be explained by the wide spread of potential across the array resulting in small changes in phase. Videos of the time evolution of the response, phase gradients, and streamlines are shown (Movies S1–S6). Phase gradient plots provide another means for SSEP monitoring and may inform of changes in SSEP propagation during surgical resection.

Validation of high-quality recordings with smaller PtNR contacts

Our microelectrode array included a multidiameter array at the tip to investigate any diameter-dependency of the recorded SSEPs and to confirm that smaller contact diameters, necessary for high-resolution mapping, do not lead to loss of information that is otherwise captured by larger contact diameter arrays. Larger contact diameters may have higher probability to overlap with fibers responsive to stimulation and may therefore potentially produce higher amplitude responses at lower stimulation currents. The diameters included were 30 μm , 60 μm , 80 μm , 110 μm , 140 μm , 170 μm , 210 μm , 240 μm and 480 μm . The contacts were organized in two mirrored clusters of 3 contacts per diameter (Fig. 4A–B). Peak-to-peak amplitude responses from the left and right-side clusters showed stronger variation in the subdural versus epidural placement (Fig. 4C), with contacts positioned ipsilaterally to the stimulation side showing a stronger response compared to contacts positioned contralaterally. For example, epidurally, 30 mA left median nerve stimulation resulted in the left 140 μm cluster recording $4.85 \pm 0.09 \mu\text{V}$ amplitude versus the right cluster recording $5.07 \pm 0.06 \mu\text{V}$. Subdurally, those left and right clusters recorded amplitudes of $7.26 \pm 0.06 \mu\text{V}$ and $4.09 \pm 0.15 \mu\text{V}$, respectively (Fig. 4D). Given that there was strong spatial variability across the array and the variable diameter electrodes were inherently in different locations, we could not directly compare the peak-to-peak amplitude responses. Therefore, we also evaluated the pre-stimulus baseline standard deviation for the contacts, with the assumption that this parameter should not be affected by the contact

position. We found that the baseline standard deviation did not show a conclusive diameter dependency in either the epidural or subdural placement (Fig. 4 E,F). Epidural baseline standard deviation was consistently $\sim 0.38 \mu\text{V}$ whereas subdural baseline standard deviation was $\sim 0.18 \mu\text{V}$. Finally, we computed the power spectral density (PSD) for both the epidural and subdural recordings over a 300 ms time segment after stimulus (Fig. 4 G,H). We did not see a diameter effect on the PSD, with all channels exhibiting a $1/f$ noise relationship followed by white noise. These data suggest that recording with $30 \mu\text{m}$ diameter PtNR contacts is as effective as recording with larger diameters, which further substantiates their use for high-definition mapping from the surface of the spinal cord.

Comparison to clinical IONM recordings

In subjects 5 and 6, we sought to understand how the research microelectrode recordings compared to clinical IONM recordings. Recordings from the microelectrode array could not be directly compared to those from the IONM equipment given the difference in trial numbers used to obtain the averaged traces for both. Only 30–40 trials were used in the averaging for the research grid at each current amplitude. The clinical IONM recordings needed longer stimulation trains given the lower amplitudes of responses at the scalp. As a result, the length of recording data segment that was averaged to achieve the mean traces differed between the research grid and clinical IONM data. However, a comparison could be made based on the general timeline of the surgery since any substantial changes in SSEPs were noted in the log sheet and typically lasted throughout the entire experiment recording session.

Epidural and subdural pre-resection and subdural post-resection recordings at 30 mA were compared to IONM recordings from similar timepoints in the surgery (Fig. 5). Research grid recordings showed a higher response amplitude compared to IONM recordings. For high current amplitudes, the range of response amplitudes measured with the research grid was much higher than for clinical IONM recordings, where 30 mA right median nerve stimulation resulted in a maximal $3 \mu\text{V}$ peak-to-peak amplitude response for the clinically recorded C3-C4 trace compared to microelectrode recordings of $> 8 \mu\text{V}$ and $> 6 \mu\text{V}$ responses for left and right 30 mA stimulation, respectively (Fig. 5A,B). The remaining clinical traces were only $\sim 1 \mu\text{V}$.

Although there was a loss of response to median nerve stimulation post-resection in subject 5, affecting the right side more strongly, our microelectrodes still resolved responses; however, these responses were smaller than the pre-resection amplitudes. The maximum response amplitude decreased from $10 \mu\text{V}$ to $2.5 \mu\text{V}$, whereas the clinical IONM equipment could not register a response (Fig. 5 C,D). Furthermore, the spatial variation in the responses was preserved in the microelectrode recordings. Stimulation with 30 mA resulted in clear left and right activation patterns, similar to those seen pre-resection (Fig. 5 E,F). The ability to map the functional midline was also preserved (Fig. 5G). Similarly, in subject 6, the research microelectrode recordings were of higher amplitude compared to the clinical recordings throughout the surgery (Fig. S8). These results highlight the potential of our microelectrode grids for IONM.

DISCUSSION

Currently deployed clinical spinal cord arrays are limited in usability by size. The thickness of these electrodes is at least on the scale of tens or hundreds of microns and often much thicker (29, 30, 32, 49, 50). As a result, these electrodes have poor contact with the spinal cord and record lower amplitude responses, requiring higher stimulation currents. Moreover, existing clinical microelectrodes typically have platinum contacts. Platinum has high impedance, requiring large contact diameters and resulting in low-resolution coverage. Large diameters limit the number of contacts across the circumference of the spinal cord, encumbering the isolation of the midline. The microelectrode arrays we developed address these limitations and could therefore be used for high resolution functional mapping of the spinal cord. Because our grids are fabricated on parylene, they can be much thinner (here, 6.6 μm thick) than platinum electrodes. Electrode contacts are composed of PtNRs and have much lower impedances compared to standard planar platinum contacts. The lower impedance of PtNRs enables scaling of the contact diameter while preserving excellent impedance values ($\sim 36 \text{ k}\Omega$ at 30 μm diameter) and recording capabilities, which offers the possibility of having higher density coverage.

In this study we transitioned from PEDOT:PSS to PtNR contacts, which have been shown to be more suitable for stimulation than other low-impedance microelectrode materials (38, 39). Although we do not perform stimulation in this study, having spinal cord electrodes that can both record and stimulate would be the goal for many applications outside of neuromonitoring. The current iteration was a recording electrode only, but a hybrid version of record and stimulate electrode is currently under development, where one or a subset of channels deliver the stimulation and the remaining channels record. This, combined with a more robust fabrication process (see Materials and Methods), suggests that PtNR microelectrodes can be a good choice for human neural devices. Our grid was 6 mm wide, as recommended by the surgical team that performed the research in the clinical setting on the first 3 subjects. For 2 out of the last 3 subjects, we were able to identify the midline and in the third, we could not. Increasing the width of the array and its axial coverage may aid isolation of the midline across diverse subjects.

The advantageous design of our research microelectrode allowed us to discriminate stimulation currents at and above 7.5 mA. This is important since 30 mA stimulation, as was used in subject 5, is considered high and may cause a pain response. In general, currents over 10 mA are considered potentially painful (51). Therefore, reducing IONM current below this amplitude may benefit the patient by reducing anesthesia interventions during a procedure. However, systematic studies for correlating current amplitudes necessary for capturing when and where neural deficits occur in dorsal fibers can be formed are yet to be conducted.

Epidural and subdural recordings showed different spatiotemporal features, which means these placements could offer distinct applications. These differences are important given that epidural placement is easier to achieve and is less invasive. Epidural placement showed peak-to-peak response amplitudes generally on par with subdural placement. However, there was less localization of responses across the array, resulting in an incoherent phase

gradient. Surgery that requires identification of the functional midline inherently involves exposure of the dorsal spinal cord and subdural clinical procedures. Therefore, the subdural microelectrode array placement can be a valuable asset for making clinical decisions in such applications because of the high-resolution identification of the functional midline and phase gradients in 2D. On the other hand, although epidural placements cannot resolve spatial variations in the response, they could be informative for evaluating the quality of the response (whether it is present and to what extent), even when IONM responses cannot be detected. This is particularly important for decompression and other surgeries that do not involve opening of the dura mater.

Our research grid was superior compared to the clinical equipment in terms of the sensitivity of the system. We averaged 30–40 trials to achieve the mean peak-to-peak amplitude responses at a stimulation rate of 2.78 Hz, therefore requiring 10–14 seconds of recorded data. The clinical equipment stimulates at 1.41 Hz, requires over 300 trials, and often throws out trials, resulting in a necessary data segment of 4 minutes or more. This is a large improvement in responsiveness of the system and could allow for quicker detection of neurological damage. In addition, at high current amplitudes, even fewer trials would be necessary with our microelectrode, resulting in practically real-time responsiveness to surgical intervention. In subject 5, we were also able to capture SSEPs with our research microelectrode when the clinical IONM system could not. This subject showed temporary neurological deficit after surgery that quickly improved, which validates that the persistent responses seen by our microelectrode carry clinical value.

There were a few limitations to this study. First, the electrode location varied between subjects since surgery was performed at different heights of the cervical spinal cord. This made it impossible to directly compare recordings between subjects. The electrode was also placed in the vicinity of abnormal tumor tissue, which further increased the variability in recordings among patients. Additionally, there was slight variation in electrode impedances and the distribution of working channels between electrodes, which introduced more variability in the datasets. Nonetheless, the overall features of the responses were consistent, including response amplitudes, propagation velocity, midline mapping capability and epidural and subdural recording of spatiotemporal differences. Another limitation of this study was the inability to directly compare the clinical grid recordings and the microelectrode recordings due to different trial numbers used to produce the mean responses. Future studies will need to investigate and quantify these differences more thoroughly. Finally, this study included only six patients, with just one patient showing a decrease in SSEP amplitude during surgery. More patients need to be included in future studies to investigate the consistency in the research microelectrode performance and its ability to better detect neurological damage compared to existing IONM equipment.

This study was approved to be performed during operative pauses, and another limitation of this study was the inability to record during the surgical resection, which is a requirement for any IONM system. To address this limitation, we are developing microelectrodes that can surround but still leave access to the resection zone, creating a ‘window in a grid’ that will allow surgical procedures to proceed while providing real-time monitoring of spatiotemporal SSEP patterns from the dorsal surface of the spinal cord. The ‘window in a grid’ electrode

would provide coverage to the rostral and caudal segments of the spinal cord to the surgical plane, thus allowing direct comparison of SSEPs below and above the surgical site. With these improvements in place, our microelectrode system could become a complete and highly detailed IONM system. Furthermore, the PtNR microelectrode grid could be used for more traditional DC mapping given its stimulation capabilities (37).

In addition to IONM, we believe our PtNR microelectrodes have implications for the treatment of SCI by providing a high-resolution, high-coverage spinal cord grid. We speculate that our research grid could potentially be used to capture sensory information from the peripheral nerves below the point of injury to be relayed to the brain, which has been pursued recently (52–54), and provide the means for targeted sensory nerve stimulation. For this, further developments will need to be made to capture native sensory pathway neural activity as opposed to recording stimulated SSEPs and to perform stimulation with PtNR electrodes. Finally, we also believe our microelectrode array could mediate SCI treatment by identifying and stimulating the root entry zones in SCI patients, which has been shown recently to restore motor function (55).

In summary, we introduce a, high-density microelectrode grid and demonstrate its ability to outperform standard clinical IONM during spinal cord surgery. For both subdural and epidural placements, we evaluated stimulation responses that were present even when IONM did not resolve any responses. Our microelectrode was able to capture detailed spatiotemporal patterns of responses that can define with high precision the 2D maps of the functional midline during surgery. Our use of this grid in high-resolution mapping from the surface of the spinal cord shows that this microelectrode holds the promise for applications that may help neurosurgical procedures and neuromodulation therapies in the spinal cord and beyond.

MATERIALS AND METHODS

Study design

The research objectives of this study were to (1) evaluate whether direct recordings from the human spinal cord could reduce the stimulation thresholds required to detect neurological activity and quantify this difference, (2) quantify the spatial selectivity of our high-channel count grids and their ability to localize the spinal cord functional midline, (3) evaluate the differences in epidural versus subdural recordings to determine optimal grid placement and (4) assess whether the research grid can identify neurological signal when it is classified as absent by the standard intraoperative neuromonitoring (IONM) equipment. Randomization was not performed and did not apply to our study since this is a proof-of-concept technology study.

Research grid fabrication, characterization, and sterilization

Both PEDOT:PSS and PtNR research grids were fabricated on 7" × 7" × 0.06" photomask-grade soda lime glass plate (Nanofilm), which were cleaned via O₂ plasma at 200 W for 5 minutes. Diluted Micro 90 (0.1%) was spincoated onto the glass plate to act as a release layer, after which the plate was coated with 3.7- μ m-thick-parylene C using a parylene

deposition system (Specialty Coating Systems 2010 Labcoater). Next, two layers of gold traces (10 nm Cr, 250 nm Au) were deposited onto the plate using standard lithography techniques and AZ5214E-IR photoresist (MicroChemicals). This double layer of leads was found to improve device yield by reducing chance of disconnects due to particles during the photolithography process.

PEDOT:PSS grid fabrication.—For PEDOT:PSS grids, the metal traces were then encapsulated in 2nd and 3rd parylene layers, each 3.1 μm thick. Concentrated Micro-90 (100μL in 50 mL DI) was spincoated before the 3rd parylene coating to allow for peel-off of this layer at a later step. Via (hole) through the parylene was performed via oxygen etching at 200 W for 39 minutes. PEDOT:PSS solution was spincoated onto the exposed contacts, cured at 150 °C for 60 min, and the 3rd parylene layer was then peeled off. The electrodes were laser cut and lifted off with DI water. Preparation of the PEDOT:PSS solution and more fabrication details can be found in previous publications, including (39).

PtNR grid fabrication.—Platinum nanorod (PtNR) contact formation on parylene C were prepared using a technique previously developed and described in our lab (40). Briefly, the metal traces and PtAg alloyed contacts were encapsulated in a second 3.1 μm parylene layer. After deposition of a Ti hard mask, the PtAg contacts and connector pads were exposed using a dry etch of the Ti layer with SF₆/Ar gas followed by oxygen dry etching of the parylene C. The samples were lifted off with 6:1 buffered oxide etchant (BOE) and the PtAg was dealloyed in 60°C nitric acid for 2 min, thereby forming the PtNRs with Pt/Ag composition of approximately 95%/5%. The microelectrodes were bonded to custom-made extender PCBs as described in a previous publication (40).

The quality of the fabricated devices and their PEDOT:PSS or PtNR contacts were first evaluated using optical microscopy. Impedance magnitude and phase at 1kHz was then measured to ensure device functionality. If the devices had high yield, they were sent for sterilization to UCSD's or OHSU's sterilization facility. The sterilization processes used were steam with gravity mode at 121°C for 30 min for PEDOT:PSS electrodes and Sterrad with the default sterilization mode for PtNR electrodes.

Subjects and research grid placement

The research subjects were patients undergoing an intramedullary spinal cord tumor resection or biopsy procedure at the cervical segment with IONM with both epidural and subdural spinal cord exposure. Subjects were recruited by the neurosurgery team involved in this study. All patients voluntarily participated after informed consent in accordance with the University of California Institutional Review Board (IRB). Subjects were informed that participating in the study would not affect the treatment they received. Participants could withdraw at any time. Recordings were acquired from 6 participants.

Surgery proceeded as normal until epidural spinal cord exposure. During the surgical exposure, the recording equipment was set up on the non-sterile side of the operating room. The research grid was removed from the sterile tray by a scrubbed-in member of the neurosurgery team. A Squate Sterile Drape (Medtronic 01-0020) was used to interface between the sterile and non-sterile recording elements. The extender board of the research

grid was inserted through an opening in the drape and touch-proof connectors of a sterile twisted pair of subdermal needle electrodes were inserted through another hole. Two Tegaderm films (3M) were taped together to seal the openings. A member of the research team then connected the extender board and the recording equipment. The research grid was then placed in sterile saline solution in a kidney dish until the recording started. Impedance was measured to ensure proper equipment connection and grid viability after sterilization. Further details are described in (40).

Data collection

Recordings were taken at three timepoints in the surgery: (1) epidurally after spinal cord exposure, (2) subdurally, on the pial surface, before tumor resection or biopsy, and (3) subdurally after tumor resection or biopsy. Impedances were measured and plotted before each recording in both sterile saline and on the spinal cord itself to check for electrode damage and equipment connectivity issues. The total recording time for all three timepoints did not exceed 30 minutes during downtime of the surgery, so as not to cause adverse effects to the patient and surgical outcome. Recordings were collected using Intan's RHD Recording Controller at 20 kHz sampling rate. A member of the research team dictated stimulation amplitude and location to the neuromonitoring team member. Notes were taken during stimulation to note approximate stimulation time and amplitude in the recording. Reference and ground needles for the research microelectrode were placed in nearby tissue. The clinical IONM system used to capture data from subjects 5 and 6 was Cascade's IOMAX.

Data processing

Research grid data was processed in MATLAB. Data was filtered to remove 60 Hz noise and harmonics using a notch filter. Data was then bandpass filtered 30–300 Hz. The low frequency was chosen to be 30 Hz to remove changes in voltage due to DC voltage shifts and ECG artifact, which was below 30 Hz, while preserving the response frequency bandwidth (a spectrogram showed responses in the frequency range of 70–150 Hz). Stimulus artifacts from the non-filtered data were used to determine stimulation timepoints and these timepoints were compared to a custom-made stimulation artifact capture system for initial experiments, but this was found to be redundant for later experiments. Notes taken during surgery were used to classify each stimulus train based on the stimulation amplitude and location. Responses were computed by averaging a 20 ms time window after each stimulus artifact. Baseline data was computed by averaging a 20 ms time window within 20–80 ms before stimulus artifact. The onset of the time window varied between stimulations and was chosen to ensure no aberrant signals were present in the baseline recording. Baseline values were then subtracted from the averaged responses. Peak-to-peak amplitude was calculated by taking the difference between the highest and lowest data points in the time window 5–20 ms after stimulus and within the 20 ms time window for baseline. The clinical data was downloaded from the IONM software IOMAX (Cascade) in the form of a .json file after the case. The data was bandpass filtered 30–750 Hz. The data was imported and plotted in Python along with corresponding timestamps and event notes from the IONM team.

Midline mapping

A signal-to-noise (SNR) thresholding technique was used to evaluate the functional midline. The mean and standard deviation of the baseline peak-to-peak amplitude was calculated. For both left- and right-side stimulation, peak-to-peak amplitudes of the response with root mean squared (RMS) numbers less than a certain value were zeroed (Equation 1), thus creating individual threshold maps for each side. For subject 5, the value of 13 was arbitrarily chosen for the subdural recording based on the number of channels that did not meet this criterium. The value of 18 was chosen for the epidural recording. The left- and right-side threshold maps were combined by taking the square root of the sum of squared thresholds (Equation 2).

$$\text{find}\left(\frac{\text{intensities} - m}{std}\right) < val = 0 \quad \text{Equation 1}$$

$$\sqrt{\text{intensities}_{right}^2 + \text{intensities}_{left}^2} = \text{combined intensities} \quad \text{Equation 2}$$

Phase gradient analysis

The spatial phase gradient of the responses was calculated in MATLAB based on previous methods described in literature (40, 56, 57). The streamlines were generated with the streamline MATLAB function to illustrate the general directional trends of the local spatial phase gradient.

Statistical analysis

We used the Welch's test to determine whether there was a significant change in impedance after Sterrad sterilization since we assumed unequal variance between samples.

We used the Mann Whitney U test to evaluate statistical significance of the peak-to-peak amplitude responses. This nonparametric test was chosen since the amplitude distributions for each current amplitude deviated slightly from a normal distribution, making a nonparametric test more appropriate. Response peak-to-peak amplitudes were compared against baseline peak-to-peak amplitudes. In each statistical test, the channels in the top 20% based on SNR were used to ensure that the significance was not affected by non-responsive channels. The Z-score was used to evaluate effect size, which is appropriate for nonparametric data, and multiple test correction was applied to the p-values since multiple tests were performed to evaluate various current amplitudes and stimulation points. Effect size was calculated by dividing the Z-score by the square root of the number of pairs (Equation 3). The Z-score was calculated in Python from the U statistic (Equation 4). P-values were corrected using the Holm method.

$$\text{effect size} = \frac{Z}{\sqrt{n}} \text{ where } n = \text{number of pairs} \quad \text{Equation 3}$$

$$Z = \frac{U - n^2/2 + 0.5}{\sqrt{n^2*(N+1)/12}}$$
Equation 4

Supplementary Material

Refer to Web version on PubMed Central for supplementary material.

Acknowledgements

The authors acknowledge insightful discussions with Prof. Tony Yakish and Dr. Sang Heon Lee of UC San Diego. The authors are grateful for the technical support from the nano3 cleanroom facilities at UC San Diego's Qualcomm Institute where the PtNRGrid fabrication was conducted. This work was performed in part at the San Diego Nanotechnology Infrastructure (SDNI) of UC San Diego, a member of the National Nanotechnology Coordinated Infrastructure, which is supported by the National Science Foundation (Grant ECCS1542148).

Funding

This work was supported by a 2018 Galvanizing Engineering in Medicine award from the UC San Diego's Altman Clinical and Translational Research Institute to S.A.D., J.C. and J.M., the National Institutes of Health Award No. NIBIB DP2-EB029757 to S.A.D., NIH BRAIN Initiative R01NS123655-01 to S.A.D. and UG3NS123723-01 to S.A.D. and the National Science Foundation (NSF) Awards No. 1728497 to S.A.D. and CAREER No. 1351980 to S.A.D., and by an NSF Graduate Research Fellowship Program No. DGE-1650112 to A.M.B. and an NIH F32 MH120886-01 to D.R.C. Any opinions, findings, and conclusions or recommendations expressed in this material are those of the author(s) and do not necessarily reflect the views of the funding agencies.

Data and materials availability:

All data obtained in this study are either presented in the paper and supplementary materials or deposited in open database. The human spinal recording data can be accessed in Data Archive BRAIN Initiative (DABI) (<https://dabi.loni.usc.edu/>). Custom Matlab codes (version R2021a) in combination with open source automatic IID detection (<http://www.ieeg.org>) and propagating wave (<https://mullerlab.github.io/>) codes were used for the analyses and is available in GitHub (<https://srussman.github.io/>).

REFERENCES

1. Cooper PR, Outcome after Operative Treatment of Intramedullary Spinal Cord Tumors in Adults: Intermediate and Long-Term Results in 51 Patients. *Neurosurgery*. 25 (1989), doi:10.1227/00006123-198912000-00001.
2. Chang SH, Park YG, Kim DH, Yoon SY, Monitoring of motor and somatosensory evoked potentials during spine surgery: Intraoperative changes and postoperative outcomes. *Annals of Rehabilitation Medicine*. 40, 470–480 (2016). [PubMed: 27446784]
3. Ng Z, Ng S, Nga V, Teo K, Lwin S, Ning C, Yeo TT, Intradural Spinal Tumors—Review of Postoperative Outcomes Comparing Intramedullary and Extramedullary Tumors from a Single Institution's Experience. *World Neurosurgery*. 109, e229–e232 (2018). [PubMed: 28974413]
4. Raco A, Esposito V, Lenzi J, Piccirilli M, Delfini R, Cantore G, Long-term follow-up of intramedullary spinal cord tumors: A series of 202 cases. *Neurosurgery*. 56, 972–979 (2005). [PubMed: 15854245]
5. Tobin MK, Geraghty JR, Engelhard HH, Linninger AA, Mehta AI, Intramedullary spinal cord tumors: A review of current and future treatment strategies. *Neurosurgical Focus*. 39, E14 (2015).
6. Verla T, Fridley JS, Khan AB, Mayer RR, Omeis I, Neuromonitoring for Intramedullary Spinal Cord Tumor Surgery. *World Neurosurgery*. 95 (2016), pp. 108–116. [PubMed: 27474459]

7. Rijs K, Klimek M, Scheltens-de Boer M, Biesheuvel K, Harhangi BS, Intraoperative Neuromonitoring in Patients with Intramedullary Spinal Cord Tumor: A Systematic Review, Meta-Analysis, and Case Series. *World Neurosurgery*. 125 (2019), pp. 498–510.e2. [PubMed: 30659972]
8. Nuwer MR, Dawson EG, Carlson LG, Kanim LEA, Sherman JD, “Somatosensory evoked potential spinal cord monitoring reduces neurologic deficits after scoliosis surgery: results of a large multicenter survey” (1995).
9. Sandalcioglu IE, Gasser T, Asgari S, Lazorisak A, Engelhorn T, Egelhof T, Stolke D, Wiedemayer H, Functional outcome after surgical treatment of intramedullary spinal cord tumors: Experience with 78 patients. *Spinal Cord*. 43, 34–41 (2005). [PubMed: 15326473]
10. Jin SH, Chung CK, Kim CH, Choi YD, Kwak G, Kim BE, Multimodal intraoperative monitoring during intramedullary spinal cord tumor surgery. *Acta Neurochirurgica*. 157, 2149–2155 (2015). [PubMed: 26446854]
11. Deletis V, Sala F, Intraoperative neurophysiological monitoring of the spinal cord during spinal cord and spine surgery: A review focus on the corticospinal tracts. *Clinical Neurophysiology*. 119 (2008), pp. 248–264. [PubMed: 18053764]
12. Gonzalez AA, Jeyanandarajan D, Hansen C, Zada G, Hsieh PC, Intraoperative neurophysiological monitoring during spine surgery: A review. *Neurosurgical Focus*. 27 (2009), doi:10.3171/2009.8.FOCUS09150.
13. MacDonald DB, Dong C, Quatralo R, Sala F, Skinner S, Soto F, Szelényi A, Recommendations of the International Society of Intraoperative Neurophysiology for intraoperative somatosensory evoked potentials. *Clinical Neurophysiology*. 130 (2019), pp. 161–179. [PubMed: 30470625]
14. Møller AR, Ansari S, Cohen-Gadol AA, Techniques of intraoperative monitoring for spinal cord function: Their past, present, and future directions. *Neurological Research*. 33, 363–370 (2011). [PubMed: 21535935]
15. Sala F, Bricolo A, Faccioli F, Lanteri P, Gerosa M, “Surgery for intramedullary spinal cord tumors: The role of intraoperative (neurophysiological) monitoring” in *European Spine Journal* (2007), vol. 16.
16. Weigang E, Hartert M, Sircar R, v Samson P, Pitzer K, Genstorfer J, Zentner J, Beyersdorf F, Setup of Neurophysiological Monitoring with tMEP/SSEP During Thoracoabdominal Aneurysm Repair. *Thorac Cardiovasc Surg*. Feb, 28–32 (2005).
17. Singh H, Vogel RW, Lober RM, Doan AT, Matsumoto CI, Kenning TJ, Evans JJ, Intraoperative Neurophysiological Monitoring for Endoscopic Endonasal Approaches to the Skull Base: A Technical Guide. *Scientifica (Cairo)*. 2016 (2016), doi:10.1155/2016/1751245.
18. Yamada T, Somatosensory Evoked Potentials. *Encyclopedia of the Neurological Sciences*, 230–238 (2014).
19. Padberg AM, Bridwell KH, SPINAL CORD MONITORING. *Orthopedic Clinics of North America* 30 (1999), doi:10.1016/S0030-5898(05)70095-X.
20. (Enno) Freye E, *Cerebral monitoring in the OR and ICU* (Springer, 2005).
21. Moller Aage, *Intraoperative Neurophysiological Monitoring* (Springer, ed. 3rd, 2010).
22. Hilibrand AS, Schwartz DM, Sethuraman V, Vaccaro AR, Albert TJ, “Comparison of Transcranial Electric Motor and Somatosensory Evoked Potential Monitoring During Cervical Spine Surgery” (2004), (available at <http://journals.lww.com/jbjsjournal>).
23. Kimchi G, Knoller N, Korn A, Eyal-Mazuz Y, Sapir Y, Peled A, Harel R, Delayed variations in the diagnostic accuracy of intraoperative neuromonitoring in the resection of intramedullary spinal cord tumors. *Neurosurgical Focus*. 50, 1–7 (2021).
24. Lesser RP, Raudzens P, Liiders H, “ Nuwer MR, Goldie WD, Morris HH, “ Dinner DS, “ Klem G, Hahn JF, Shetter AG, Ginsburg HH, Gurd AR, Postoperative Neurological Deficits May Occur Despite Unchanged Somatosensory Evoked Potentials T Intraoperatve. *Annals of Neurology*. 19, 22–25 (1986). [PubMed: 3947036]
25. Kelleher MO, Tan G, Sarjeant R, Fehlings MG, Predictive value of intraoperative neurophysiological monitoring during cervical spine surgery: A prospective analysis of 1055 consecutive patients. *Journal of Neurosurgery: Spine*. 8, 215–221 (2008). [PubMed: 18312072]

26. Holsheimer J, Barolat G, Struijk JJ, He J, Significance of the Spinal Cord Position in Spinal Cord Stimulation. *Advances in Stereotactic and Functional Neurosurgery* 11. *Acta Neurochirurgica Supplementum*. 64, 119–124 (1995).
27. Holsheimer J, Barolat G, Spinal Geometry and Paresthesia Coverage in Spinal Cord Stimulation. *Neuromodulation: Technology at the Neural Interface*. 1, 129–136 (1998). [PubMed: 22150980]
28. Mehta AI, Mohrhaus CA, Husain AM, Karikari IO, Hughes B, Hodges T, Gottfried O, Bagley CA, Dorsal Column Mapping for Intramedullary Spinal Cord Tumor Resection Decreases Dorsal Column Dysfunction. *Journal of Spinal Disorders & Techniques*. 25 (2012), doi:10.1097/BSD.0b013e318215953f.
29. Yanni DS, Ulkatan S, Deletis V, Barrenechea IJ, Sen C, Perin NI, Utility of neurophysiological monitoring using dorsal column mapping in intramedullary spinal cord surgery. *Journal of Neurosurgery: Spine*. 12 (2010), doi:10.3171/2010.1.SPINE09112.
30. Deletis V, Sala F, “The Role of Intraoperative Neurophysiology in the Protection or Documentation of Surgically Induced Injury to the Spinal Cord.”
31. Nair D, Kumaraswamy VM, Braver D, Kilbride RD, Borges LF, Simon M. v., Dorsal column mapping via phase reversal method: The refined technique and clinical applications. *Neurosurgery*. 74, 437–446 (2014). [PubMed: 24448182]
32. Quinones-Hinojosa A, Gulati M, Lyon R, Gupta N, Yingling C, Spinal Cord Mapping as an Adjunct for Resection of Intramedullary Tumors: Surgical Technique with Case Illustrations. *Neurosurgery*. 51 (2002), doi:10.1097/00006123-200211000-00015.
33. Hermiz J, Hossain L, Arneodo EM, Ganji M, Rogers N, Vahidi N, Halgren E, Gentner TQ, Dayeh SA, Gilja V, Stimulus Driven Single Unit Activity From Micro-Electrocorticography. *Frontiers in Neuroscience*. 14 (2020), doi:10.3389/fnins.2020.00055.
34. Yang JC, Paulk AC, Salami P, Lee SH, Ganji M, Soper DJ, Cleary D, Simon M, Maus D, Lee JW, Nahed B. v., Jones PS, Cahill DP, Cosgrove GR, Chu CJ, Williams Z, Halgren E, Dayeh S, Cash SS, Microscale dynamics of electrophysiological markers of epilepsy. *Clinical Neurophysiology*. 132, 2916–2931 (2021). [PubMed: 34419344]
35. Ganji M, Kaestner E, Hermiz J, Rogers N, Tanaka A, Cleary D, Lee SH, Snider J, Halgren M, Cosgrove GR, Carter BS, Barba D, Uguz I, Malliaras GG, Cash SS, Gilja V, Halgren E, Dayeh SA, Development and Translation of PEDOT:PSS Microelectrodes for Intraoperative Monitoring. *Advanced Functional Materials*. 28 (2018), doi:10.1002/adfm.201700232.
36. Paulk AC, Yang JC, Cleary DR, Soper DJ, Halgren M, O'Donnell AR, Lee SH, Ganji M, Ro YG, Oh H, Hossain L, Lee J, Tchoe Y, Rogers N, Kiliç K, Ryu SB, Lee SW, Hermiz J, Gilja V, Ulbert I, Fabó D, Thesen T, Doyle WK, Devinsky O, Madsen JR, Schomer DL, Eskandar EN, Lee JW, Maus D, Devor A, Fried SI, Jones PS, Nahed B. v., Ben-Haim S, Bick SK, Richardson RM, Raslan AM, Siler DA, Cahill DP, Williams ZM, Cosgrove GR, Dayeh SA, Cash SS, Microscale Physiological Events on the Human Cortical Surface. *Cereb Cortex*. 31, 3678–3700 (2021). [PubMed: 33749727]
37. Ganji M, Paulk AC, Yang JC, Vahidi NW, Lee SH, Liu R, Hossain L, Arneodo EM, Thunemann M, Shigyo M, Tanaka A, Ryu SB, Lee SW, Tchoe Y, Marsala M, Devor A, Cleary DR, Martin JR, Oh H, Gilja V, Gentner TQ, Fried SI, Halgren E, Cash SS, Dayeh SA, Selective Formation of Porous Pt Nanorods for Highly Electrochemically Efficient Neural Electrode Interfaces. *Nano Letters*. 19, 6244–6254 (2019). [PubMed: 31369283]
38. Ganji M, Hossain L, Tanaka A, Thunemann M, Halgren E, Devor A, Dayeh SA, Ganji M, Dayeh SA, Hossain L, Tanaka A, Thunemann M, Monolithic and Scalable Au Nanorod Substrates Improve PEDOT-Metal Adhesion and Stability in Neural Electrodes, doi:10.1002/((please).
39. Ganji M, Tanaka A, Gilja V, Halgren E, Dayeh SA, Scaling Effects on the Electrochemical Stimulation Performance of Au, Pt, and PEDOT:PSS Electrocorticography Arrays. *Advanced Functional Materials*. 27 (2017), doi:10.1002/adfm.201703019.
40. Tchoe Y, Bourhis AM, Cleary DR, Stedelin B, Lee J, Tonsfeldt KJ, Brown EC, Siler D, Paulk AC, Yang JC, Oh H, Goo Ro Y, Lee K, Russman S, Ganji M, Galton I, Ben-Haim S, Raslan AM, Dayeh SA, Human brain mapping with multithousand-channel PtNRGrids resolves spatiotemporal dynamics. *Science Translational Medicine*, 1441 (2022).

41. Vatsyayan R, Cleary D, Martin JR, Halgren E, Dayeh SA, Electrochemical safety limits for clinical stimulation investigated using depth and strip electrodes in the pig brain. *Journal of Neural Engineering*. 18 (2021), doi:10.1088/1741-2552/ac038b.
42. MacDonald DB, Skinner S, Shils J, Yingling C, Intraoperative motor evoked potential monitoring - A position statement by the American Society of Neurophysiological Monitoring. *Clinical Neurophysiology*. 124 (2013), pp. 2291–2316. [PubMed: 24055297]
43. Deletis V, Seidel K, “Neurophysiological identification of long sensory and motor tracts within the spinal cord” in *Neurophysiology in Neurosurgery* (Elsevier, 2020), pp. 163–175.
44. McLeod JG, Wray SH, Conduction velocity and fibre diameter of the median and ulnar nerves of the baboon. *J Neurol Neurosurg Psychiatry*. 30, 240–247 (1967). [PubMed: 4962146]
45. Eisen A, Hoirsch M, White J, Calne D, Sensory group Ia proximal conduction velocity. *Muscle & Nerve*. 7, 636–641 (1984). [PubMed: 6543910]
46. Pelosi L, Cracco JB, Cracco RQ, “Conduction characteristics of somatosensory evoked potentials to peroneal, tibial and sural nerve stimulation in man” (1987).
47. Sakatani YW,K, “Neurophysiological Mechanisms of Somatosensory-Evoked Potential Changes” in *Neural Monitoring* (Humana Press, Totowa, NJ, 1990), pp. 115–148.
48. Isakovic J, Dobbs-Dixon I, Chaudhury D, Mitrecic D, Modeling of inhomogeneous electromagnetic fields in the nervous system: a novel paradigm in understanding cell interactions, disease etiology and therapy. *Scientific Reports*. 8 (2018), doi:10.1038/s41598-018-31054-9.
49. Kržan MJ, “Intraoperative Neurophysiological Mapping of the Spinal Cord’s Dorsal Columns” in *Neurophysiology in Neurosurgery* (Elsevier, 2002).
50. Nair D, Kumaraswamy VM, Braver D, Kilbride RD, Borges LF, Simon M. v., Dorsal column mapping via phase reversal method: The refined technique and clinical applications. *Neurosurgery*. 74, 437–446 (2014). [PubMed: 24448182]
51. The Fatal Current. *Physical Therapy*. 46 (1966), doi:10.1093/ptj/46.9.968.
52. Bunday KL, Urbin MA, Perez MA, Potentiating paired corticospinal-motoneuronal plasticity after spinal cord injury. *Brain Stimulation*. 11, 1083–1092 (2018). [PubMed: 29848448]
53. Yadav AP, Li D, Nicoletis MAL, A Brain to Spine Interface for Transferring Artificial Sensory Information. *Scientific Reports*. 10 (2020), doi:10.1038/s41598-020-57617-3.
54. Yadav AP, Li S, Krucoff MO, Lebedev MA, Abd-El-Barr MM, Nicoletis MAL, Generating artificial sensations with spinal cord stimulation in primates and rodents. *bioRxiv* (2020), doi:10.1101/2020.05.09.085647.
55. Rowald A, Komi S, Demesmaeker R, Baaklini E, Hernandez-Charpak SD, Paoles E, Montanaro H, Cassara A, Becce F, Lloyd B, Newton T, Ravier J, Kinany N, D’Ercole M, Paley A, Hankov N, Varescon C, McCracken L, Vat M, Caban M, Watrin A, Jacquet C, Bole-Feysot L, Harte C, Lorach H, Galvez A, Tschopp M, Herrmann N, Wacker M, Geernaert L, Fodor I, Radevich V, van den Keybus K, Eberle G, Pralong E, Roulet M, Ledoux J-B, Fornari E, Mandija S, Mattera L, Martuzzi R, Nazarian B, Benkler S, Callegari S, Greiner N, Fuhrer B, Froeling M, Buse N, Denison T, Buschman R, Wende C, Ganty D, Bakker J, Delattre V, Lambert H, Minassian K, van den Berg CAT, Kavounoudias A, Micera S, van de Ville D, Barraud Q, Kurt E, Kuster N, Neufeld E, Capogrosso M, Asboth L, Wagner FB, Bloch J, Courtine G, Activity-dependent spinal cord neuromodulation rapidly restores trunk and leg motor functions after complete paralysis. *Nature Medicine* (2022), doi:10.1038/s41591-021-01663-5.
56. Rubino D, Robbins KA, Hatsopoulos NG, Propagating waves mediate information transfer in the motor cortex. *Nature Neuroscience*. 9, 1549–1557 (2006). [PubMed: 17115042]
57. Muller L, Piantoni G, Koller D, Cash SS, Halgren E, Sejnowski TJ, Rotating waves during human sleep spindles organize global patterns of activity that repeat precisely through the night. *Elife*. 5 (2016), doi:10.7554/eLife.17267.001.

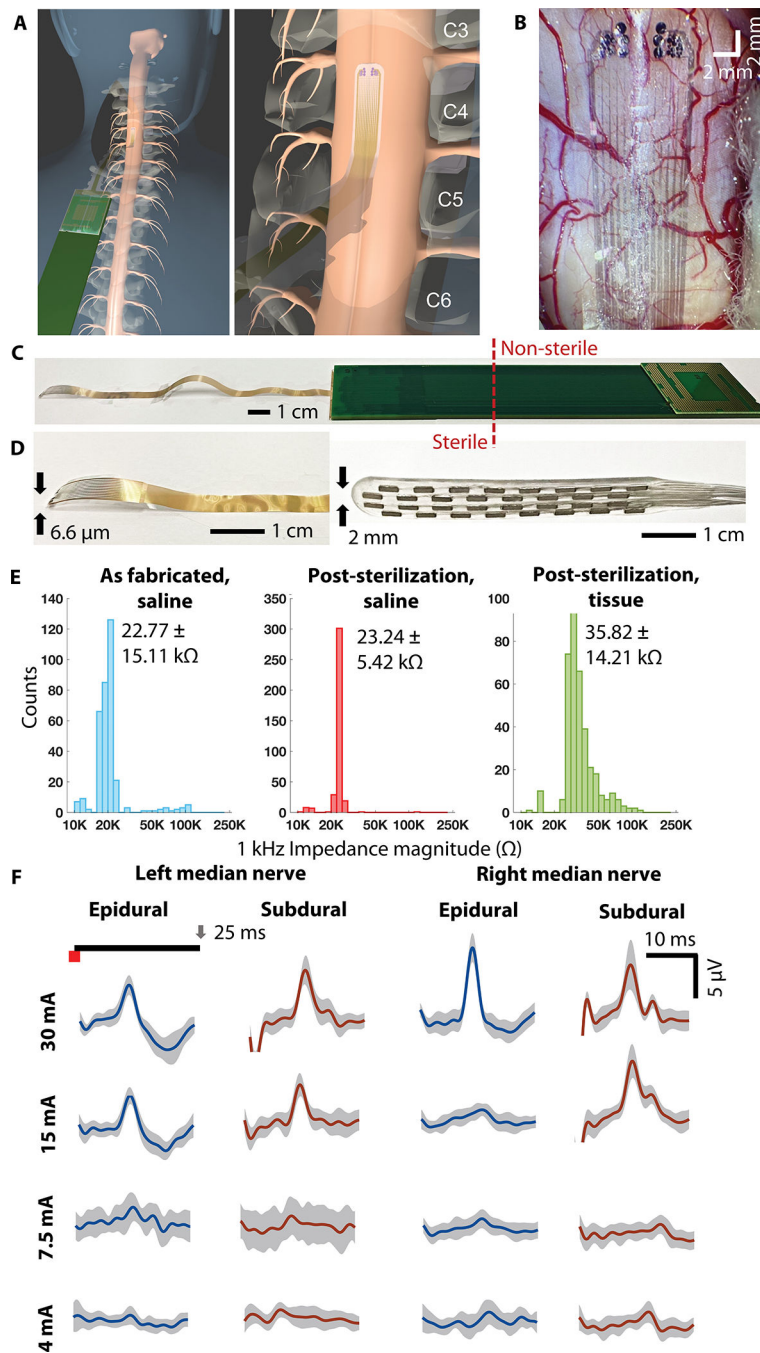


Figure 1. Experiment overview and electrode design. (A) schematic diagram of the placement of the research grid on the subject's spinal cord. (B) Photograph of the research grid placed on the subdural surface of spinal cord during recording. (C) Research microelectrode bonded to extender PCB with the sterile/non-sterile junction point highlighted. (D) Comparison of size and thickness of the research microelectrode versus a clinical grid (CoverEdge X 32, Boston Scientific). (E) 1-kHz impedance magnitude histograms measured as fabricated in saline, post-sterilization in saline, and on spinal cord tissue. (F) Example single-channel responses

to different left and right median nerve stimulation current amplitudes recorded epidurally and subdurally pre-resection. The channel with the highest peak-to-peak amplitude response was chosen as the example channel for each condition.

Author Manuscript

Author Manuscript

Author Manuscript

Author Manuscript

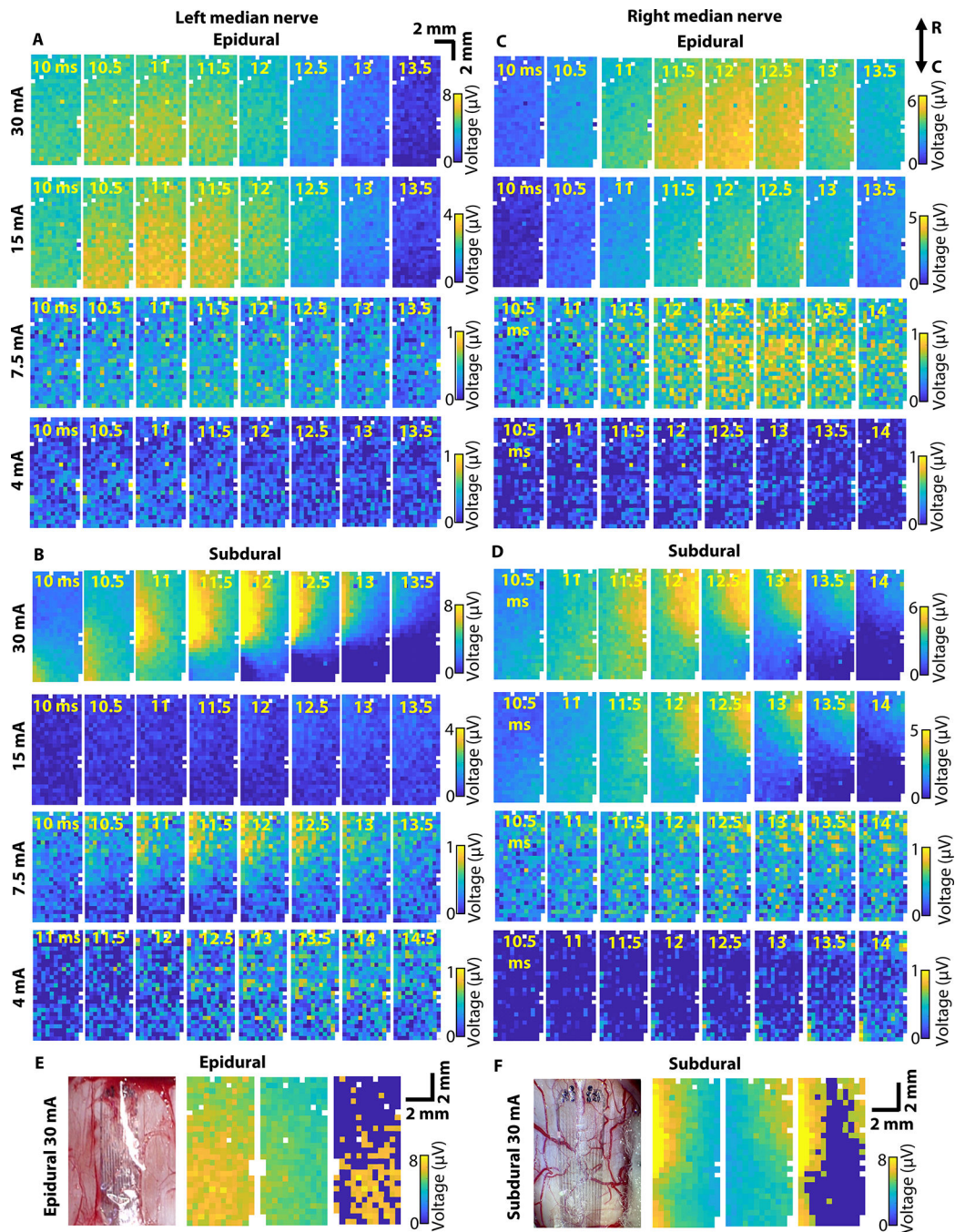


Figure 2. Time evolution plots of recorded SSEPs and functional midline mapping. (A) – (D) Spatial distribution of peak-to-peak amplitudes of responses to both left and right median nerve stimulation recorded epidurally and subdurally pre-resection. (E) Functional midline estimation from epidural recording of responses to 30 mA left and right median nerve stimulation. (F) Functional midline estimation from subdural recording of responses to 30 mA left and right median nerve stimulation. Peak-to-peak response amplitudes over the entire recording segment can be found in Fig. S3.

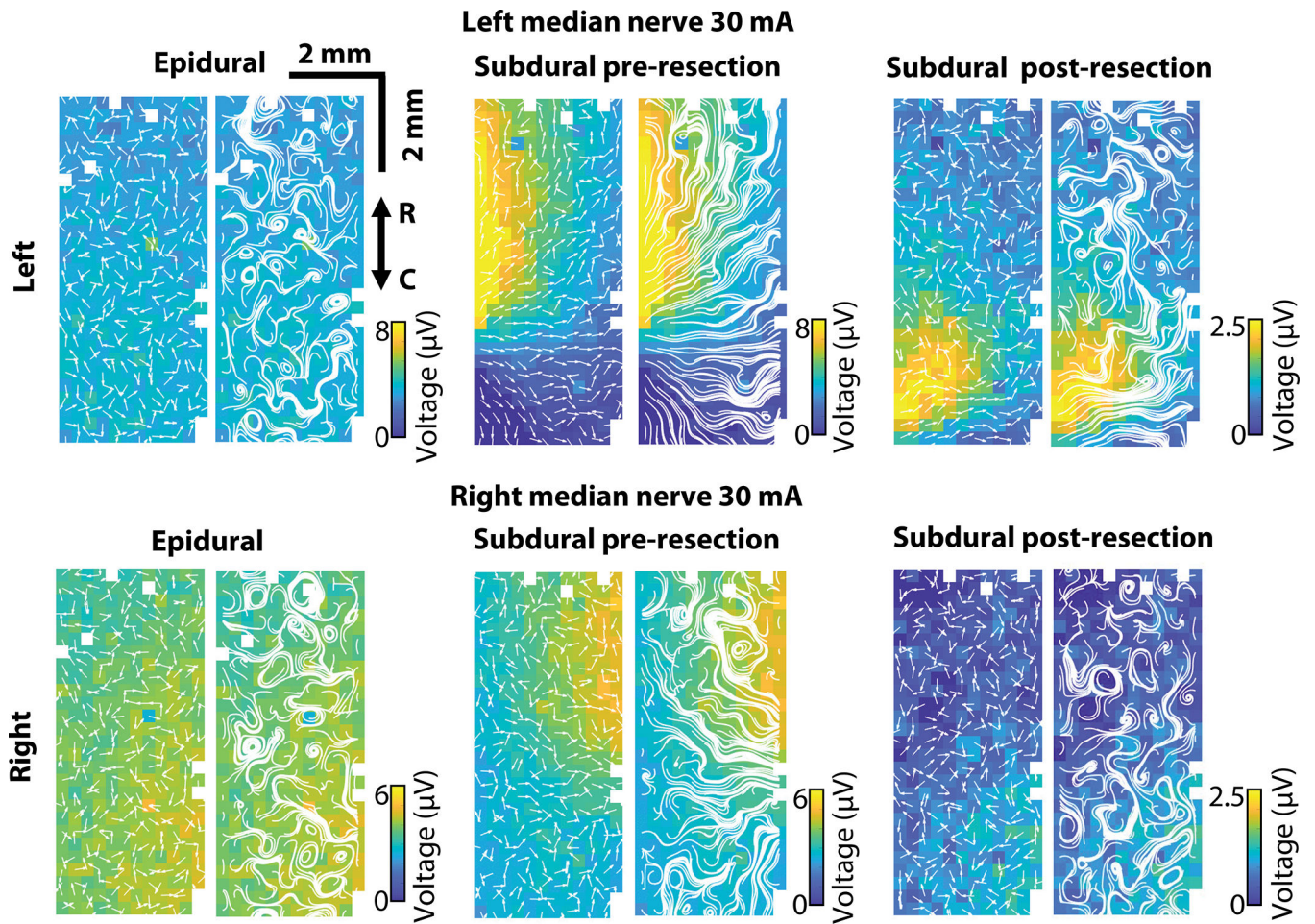


Figure 3. Spatial phase gradients and streamlines of SSEP responses. SSEP spatial phase gradients and streamlines in response to 30 mA left (top panels) and right (bottom panels) median nerve stimulation.

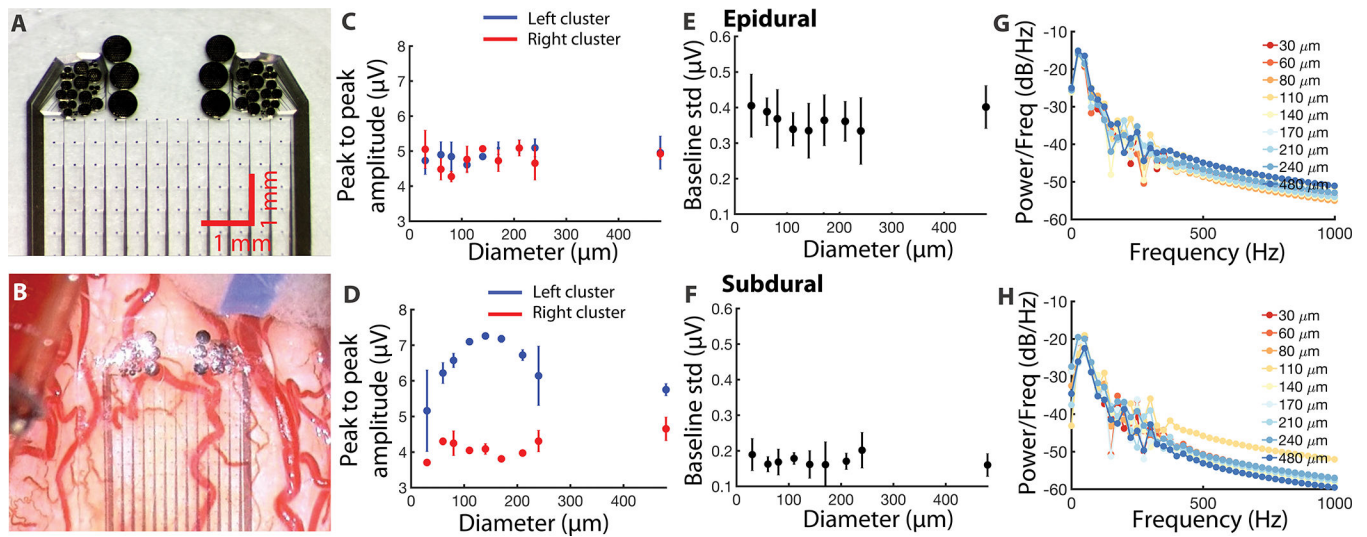


Figure 4. Multidiameter array response analysis. (A) Image of multidiameter array at tip of research microelectrode. (B) Image of electrode placed subdurally on spinal cord during recording. (C) – (D) Averaged peak-to-peak amplitude responses recorded epidurally and subdurally to 30 mA left median nerve stimulation. (E) – (F) Averaged baseline standard deviation recorded epidurally and subdurally. (G) – (H) Power spectrum density analysis on baseline recordings from (E) – (F).

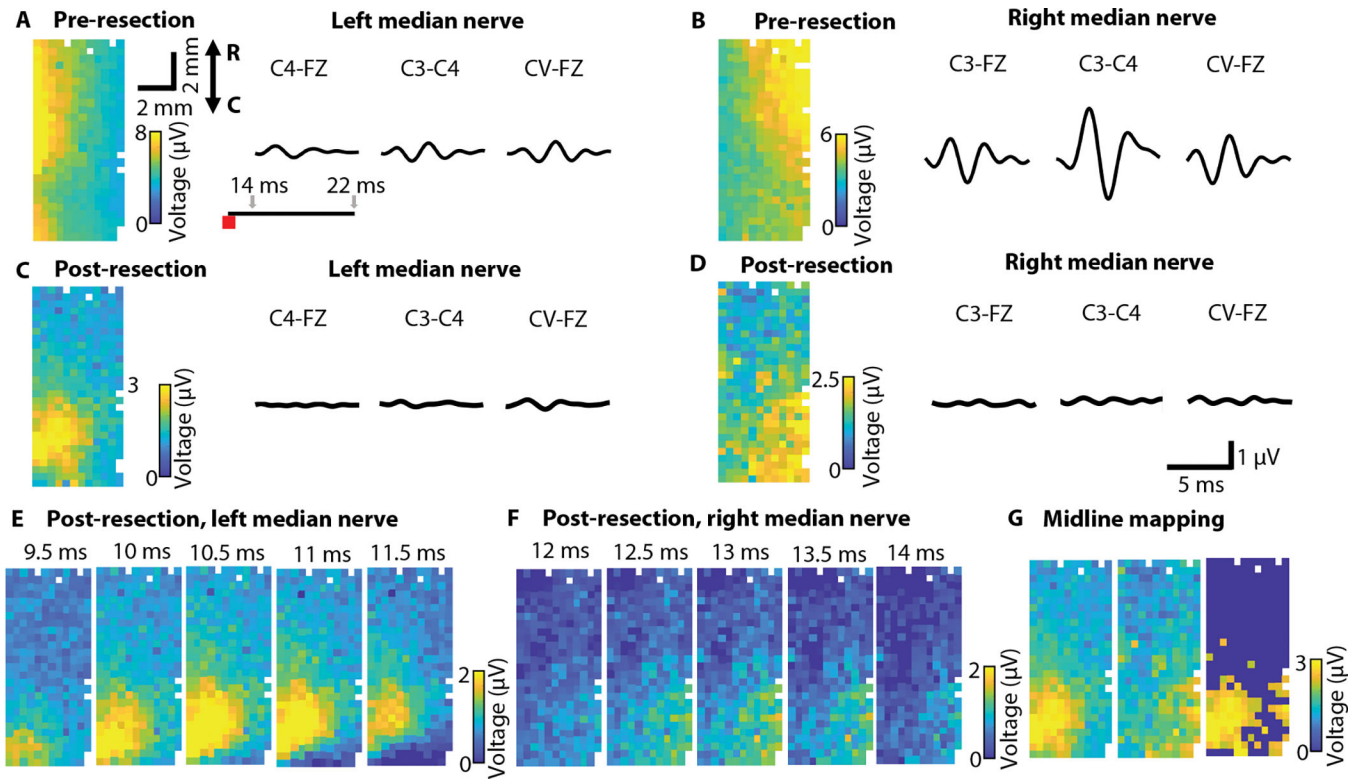


Figure 5. Comparison to clinical IONM recordings. (A) – (D) Subdural pre-resection and post-resection recordings to left and right 30 mA median nerve stimulation. (E) – (F) Time evolution of post-resection recorded responses to 30 mA left and right median nerve stimulation. (G) Functional midline estimation from post-resection recorded responses to 30 mA left and right median nerve stimulation.

Table 1.

Statistical analysis and significance of results from subject 5.

	Mean SNR	T-test	Effect size
Epidural Left			
30 mA	26.79 ± 0.93	2.45E-119	-1.73
15 mA	19.49 ± 1.29	2.45E-119	-1.73
7.5 mA	8.53 ± 2.05	1.24E-112	-1.67
4 mA	1.19 ± 0.12	4.32E-17	0.73
Epidural Right			
30 mA	14.25 ± 0.46	2.45E-119	-1.73
15 mA	18.94 ± 1.66	6.89E-119	-1.73
7.5 mA	5.11 ± 0.76	8.27E-78	-1.39
4 mA	3.00 ± 0.69	4.60E-5	0.29
Subdural Left			
30 mA	28.86 ± 2.27	7.50E-25	-1.72
15 mA	5.62 ± 1.02	7.45E-12	-1.15
7.5 mA	8.24 ± 1.71	2.53E-20	-1.54
4 mA	3.67 ± 0.82	0.0145	-1.00
Subdural Right			
30 mA	9.08 ± 0.45	7.50E-25	-1.72
15 mA	17.62 ± 3.15	5.29E-23	-1.79
7.5 mA	4.47 ± 1.05	0.275	-0.14
4 mA	4.69 ± 1.42	4.19E-4	-0.64

Author Manuscript

Author Manuscript

Author Manuscript

Author Manuscript